ChemistryOpen

Research Article
doi.org/10.1002/open.202200033

Chemistry
Europe
European Chemical
Societies Publishing

www.chemistryopen.org

Supramolecular Arrangement and DFT analysis of Zinc(II) Schiff Bases: An Insight towards the Influence of Compartmental Ligands on Binding Interaction with Protein

Megha Sen Chowdhury,[a] Selcuk Gumus,[b] Sanchari Dasgupta,[c, d] Ishani Majumder,[c] Abir Bhattacharya,*[e] Debasis Das,[c] Jayanta Mukhopadhyay,[f] Debosreeta Bose,[a] Saumya Dasgupta,*[a] Yuksel Akinay,*[g] and Madhumita Mukhopadhyay*[a, h]

We report, for the first time, a detailed crystallographic study of the supramolecular arrangement for a set of zinc(II) Schiff base complexes containing the ligand 2,6-bis((E)-((2-(dimethylamino)ethyl)imino)methyl)-4-R-phenol], where R = methyl/tert-butyl/chloro. The supramolecular study acts as a pre-screening tool for selecting the compartmental ligand R of the Schiff base for effective binding with a targeted protein, bovine serum albumin (BSA). The most stable hexagonal arrangement of the complex [Zn–Me] (R = Me) stabilises the ligand with the highest FMO energy gap ($\Delta E = 4.22$ eV) and lowest number of conformations during binding with BSA. In contrast, formation of unstable 3D columnar vertebra for [Zn–Cl] (R = Cl) tend to activate the system with lowest FMO gap (3.75 eV) with highest spontaneity factor in molecular docking. Molecular docking analyses reported in terms of 2D LigPlot+ identified site A, a cleft of domains IB, IIIA and IIIB, as the most probable protein binding site of BSA. Arg144, Glu424, Ser428, Ile455 and Lys114 form the most probable interactions irrespective of the type of compartmental ligands R of the Schiff base whereas Arg185, Glu519, His145, Ile522 act as the differentiating residues with $\Delta G = -7.3$ kcal mol^{-1}.

Introduction

Schiff bases produced by the reaction of amines and carbonyl compounds are the organic products containing –C=N– groups.[1–3] Recently, stable complexes of Schiff bases with different transition metals have attracted strong attention due to their structural properties, catalytic activities, and biological properties for magnetic, dielectric, and optical applications.[4,5] However, Schiff bases undergoes certain side reactions such as hydrolysis which leads to the formation of unwanted products.

[a] M. Sen Chowdhury, Dr. D. Bose, Dr. Saumya Dasgupta,
Dr. M. Mukhopadhyay
Department of Chemistry
Amity Institute of Applied Sciences (AIAS)
Amity University
700156 Kolkata (India)
E-mail: sdasgupta@kol.amity.edu
madhumita.mukhopadhyay@makautwb.ac.in
madhubanerji@gmail.com

[b] Dr. S. Gumus
Van Yuzuncu Yil University
Department of Chemistry
Faculty of Science
4445065 Van (Turkey)

[c] Dr. S. Dasgupta, Dr. I. Majumder, Dr. D. Das
Department of Chemistry
University of Calcutta
92, A. P. C. Road, 700 009 Kolkata, West Bengal (India)

[d] Dr. S. Dasgupta
Institut Lavoisier de Versailles
UMR CNRS 8180
Universailles St-Quentin-en-Yvelines
Universite Paris-Saclay
78035 Versailles Cedex (France)

[e] Dr. A. Bhattacharya
Department of Physics
The Bhawanipur Education Society College
University of Calcutta
700020 Kolkata (India)
E-mail: abirphs@gmail.com

[f] Dr. Jayanta Mukhopadhyay
Energy Materials & Devices Division
CSIR-Central Glass and Ceramic Research Institute
700 032 Kolkata (India)

[g] Dr. Yuksel Akinay
Van Yuzuncu Yil University
Department of Mining
Engineering Faculty
4445065 Vancity (Turkey)
E-mail: yukselakinay@gmail.com

[h] Dr. M. Mukhopadhyay
Present Affiliation:
Department of Materials Science & Technology
School of Applied Science & Technology
Maulana Abul Kalam Azad University of Technology (MAKAUT)
741249 Nadia, West Bengal (India)

Supporting information for this article is available on the WWW under
https://doi.org/10.1002/open.202200033

ChemistryOpen

Research Article
doi.org/10.1002/open.202200033

Chemistry Europe
European Chemical
Societies Publishing

These problems are dependent on the reaction conditions and co-ligand type. For practical applications, different types of metal complexes with Schiff bases have been studied to enhance their properties. Among these, Zinc (Zn) is one of the most studied metals with Schiff bases. As per the literature, Zn is the second most abundant element having various biological effects in the human body after iron. In the last decades, the Zn derived Schiff bases are extensively investigated in the field of enzyme regulation, DNA interaction, neuronal signal transmission, protein, Lewis's activation, gene expression and nucleophiles.[6–8] Shiva Krishnaloke et al. synthesized Zn diiminodipyrromethane Schiff bases complexes for in vitro cytotoxicity and antibacterial activities using cancer cells.[9] Ajmeera Ramesh et al. has reported biological activity of Schiff bases of 4-aminoantipyrine with copper(II), zinc(II), nickel(II), and cobalt(II) metals. The obtained results showed that Schiff bases of 4-aminoantipyrine with Zn metals displayed the best antimicrobial activity compared with other metal complexes ligands.[10]

In this context, the present investigation intends to study the binding interaction of an in house developed zinc(II) Schiff base with bovine serum albumin (BSA). The mentioned zinc(II) Schiff base is synthesized by Dasgupta et al.[11] with functionalization at para position with methyl (Me), isopropyl (ⁱPr), tertiary butyl (ᵗBu) and chloride (Cl) compartmental ligands. It could be observed from Figure 1, **R** position (*para* to −OH group) is replaced by variable groups (termed as compartmental ligands) as mentioned. Dasgupta et al.[11] reported the synthesis of the four zinc(II) Schiff bases and employed as an effective nitro aromatic detector upon utilising their fluorescent behaviour. In continuation, Sen Chowdhury et al.[12] reported the binding interaction among the neutral fluorophore of zinc(II) Schiff base having compartmental ligands, namely, *tert*-butyl (ᵗBu), methyl, and chloride with BSA as the bio-membrane. The primary objective is to selectively screen and apply the zinc(II) system as an Active Pharmaceutical Ingredient (API). The primary limitation of the experimental outcome in this regard is the absence of screening database with respect to the comparative reactivity of the zinc(II) system as a function of compartmental ligand. For establishing as an active API, binding interaction of the system needs to be studied with multiple targeted protein system. This would incur significant budget and critical experimentation. In this regard, the authors' aims to pursue a theoretical screening on the basis of ligand-protein interaction through molecular docking. The primary governing parameter in this regard is based on the 3D stability and reactivity of the Schiff base. The

novelty of the research work is to establish that, supramolecular arrangement of a system could predict the binding interaction with a macromolecular system like protein. In the present context, authors have undertaken the study on supramolecular arrangement of Zn-Schiff base with the said substituents of Me, ⁱPr, ᵗBu and Cl ligands. This enables a pre-screening for applicability of such biocompatible crystalline Schiff bases for variable biomimicking and protein environment. Protein, being a macromolecule possess critical and numerous binding sites for ligand binding. A series of experimental studies required to be undertaken with each substrate for establishing the efficacy. The present study, however, intend to utilize supramolecular arrangement as a tool to screen the Schiff base for effective binding with Bovine serum albumin (BSA) as the primary protein. The reactivity pattern of the system is analysed using FMO approach and substantiated with electrostatic potential maps. This has the background of predicting the crystal structures by DFT which agrees closely with the results obtained from X-Ray diffraction data.[12] Therefore, the reported can enable a pre-screening of the binding interaction of protein with the targeted Schiff base. This is supported from an initial study on supramolecular arrangement and reactivity of the Schiff base with four compartmental ligands.

Theoretical Details

As mentioned in the Introduction, the authors' aim to study the feasibility of zinc(II)-based Schiff base with functionalization at para position with methyl (Me), isopropyl (ⁱPr), *tert*-butyl (ᵗBu) and chloride (Cl) compartmental ligands as an Active Pharmaceutical Ingredient (API). In this context, molecular docking with BSA of the four systems (Table 1) forms the prime objective of the present study. The zinc(II) Schiff base with four compartmental ligands is synthesised and characterised by Dasgupta et al. and has been examined as an efficient nitro aromatic detector.[11] The representative structure of zinc(II) Schiff bases as tabulated in Table 1 are shown in Figure 1. Preliminary experiment (s) in terms of binding interaction of zinc(II) system with Cl-, Me and ᵗBu group with BSA has been reported by Sen Chowdhury et al.[12] However, the reported study lacks the interaction analysis of Schiff base with protein. In order to get established as an API, the target system needs to have various interactions (associative or inhibitory) as per the type of protein. This requires the detailed interaction analyses prior to the
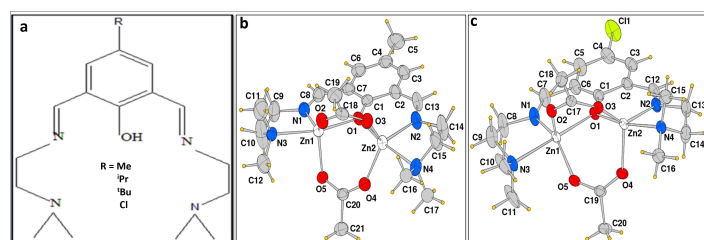
Figure 1. a) Structure of four synthesized compartmental ligands and representative structure of zinc(II) Schiff base with b) Me and c) Cl as the compartmental ligand.

ChemistryOpen

Research Article
doi.org/10.1002/open.202200033

Chemistry Europe
European Chemical
Societies Publishing

Table 1. Specification of experimental samples and sample IDs.

Name of the zinc(II) Schiff base complexes	Sample ID	Sample ID after binding with BSA
2,6-bis((E)-((2-(dimethylamino) ethyl)imino)methyl)-4-methyl-phenol	**[Zn—Me]**	BSA–L–Cl
2,6-bis((E)-((2-(dimethylamino) ethyl)imino)methyl)-4-isopropyl-phenol	**[Zn—iPr]**	BSA–L–tBu
2,6-bis((E)-((2-(dimethylamino) ethyl)imino)methyl)-4-tert-butyl-phenol	**[Zn—tBu]**	BSA–L–Me
2,6-bis((E)-((2-(dimethylamino) ethyl)imino)methyl)-4-chloro-phenol	**[Zn—Cl]**	BSA–L–iPr

experimental study. This present research article aims towards the theoretical study of such interaction using molecular docking analysis[13].

Prior to the docking analysis, a comparative analysis on the reactivity of zinc(II) system as a function of various ligands is essential. In this aspect, the authors have undertaken supramolecular analysis of targeted ligand which enables a pre-screening for applicability of such biocompatible crystalline Schiff bases for variable biomimicking and protein environment. In addition, detailed Frontier molecular orbital (FMO) analyses is reported along with requite electrostatic potential maps. Such results obtained from FMO and supramolecular patterning is well correlated with molecular docking analysis. The subsequent sections describes the details of such theoretical tools.

Supramolecular Arrangement of [Zn—Me/iPr/tBu/Cl] using Mercury 4.2.0

The utmost need to study the molecular microenvironment of the zinc(II) complexes of the Schiff bases by means of various available applications is largely to arrive at the most acceptable conclusion that how and where exactly the binding of the protein moiety takes place. The main objective lies in proper viewing and identification of the "site of binding" within the protein with the compartmental ligands of the Schiff base. The involved Schiff base complex involve numerous associations in terms of both primary and secondary interactions. This is generated owing to the presence of unsatisfied coordination sites within the parent base system.[14–16] In this connection, the functionality of secondary bond interactions viz. hydrogen, van der Waals interaction are significant which enable stronger association with selected protein(s) as described in subsequent section. Therefore, a prior quantitative knowledge on the extent of secondary bonding interaction within the Schiff bases need to be analysed in regard to affinity factor, bond energies, and others. This further requires correlation with DFT analyses and applied for understanding molecular docking studies with selected proteins. The process involves the application of Mercury 4.2.0 to precisely funnel out the desired range of secondary (mainly Hydrogen bond) interactions, and selectively expanding these contacts to obtain a satisfactory 2D and 3D supramolecular formations.

Analyses of [Zn—Me/iPr/tBu/Cl] using Density Functional Theory

Gaussian 16, Revision B.01[17] package program was used to obtain the ground state (S_0) geometries of all compounds with the application of B3LYP[18,19] hybrid functional and 6-311++G (d,p) the basis set. No symmetry restrictions were applied during geometry optimizations. The vibrational analysis did not yield any imaginary frequencies which indicate that the geometries obtained are at least a minimum on the potential energy surface. The visualization of the different structural forms of zinc(II) Schiff bases were done by Gauss View 5.0 software[16, 17]. The electronic indices such as energy of the lowest unoccupied molecular orbital (E_{LUMO}), energy of the highest occupied molecular orbital (E_{HOMO}) of the experimental system is also computed. The energies of the lowest singlet excited states (S) of the compounds were obtained via Time-Dependent Density Functional Theory (TDDFT) by the same basis set.

Molecular Docking Studies

For theoretical analysis, crystal structure of BSA was obtained from the Protein Data Bank (PDB) having PDB entry ID: 4F5S (https://www.rcsb.org/structure/4F5S). The ligand structures ([Zn—Me], [Zn—iPr], [Zn—tBu] and [Zn—Cl]) were generated by Gauss View 5.0. and their geometry was optimized using the Gaussian 09 suite of quantum chemical programs.[16] The required 3D, PDB structure of the ligand structures of the Schiff base complexes were generated by using Gauss View 5.0 after their respective geometry optimization.
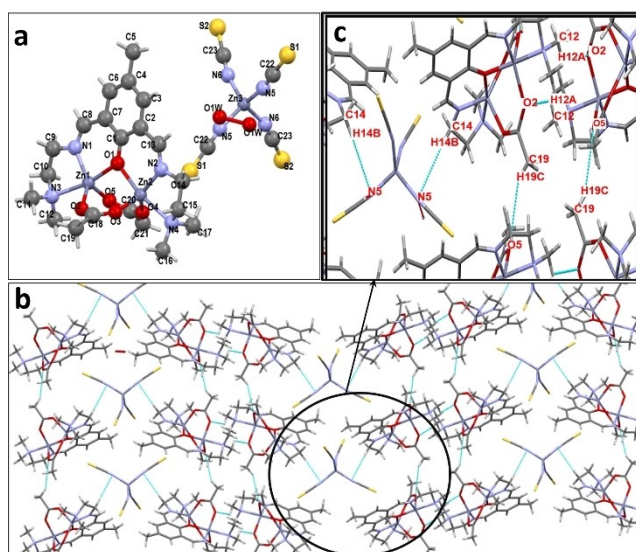
All BSA-ligand docking simulations are performed with SWISSDOCK[20] and are analysed through UCSF Chimera.[21] For each BSA-ligand pair, docking was performed in SWISSDOCK with default parameters with .pdb file of the protein and mol2 file of the ligand. For each protein-ligand pair, the docking-type was found to be exact and rigid. All predicted binding modes are scored in terms of the corresponding parameters like 'Full Fitness value', 'ΔG', and others. All binding modes were carefully visualized by UCSF Chimera for further analysis.

ChemistryOpen

Research Article
doi.org/10.1002/open.202200033

**Chemistry
Europe**
European Chemical
Societies Publishing

Results and Discussion

Effect of Compartmental Ligands on the Crystallographic and Supramolecular Assembly of Zinc(II) Schiff Base

The primary aim of the present investigation is to analyse the influence of compartmental ligands (i.e., *para* substituents) on the binding interaction of protein (BSA) with zinc(II) Schiff base. For such analyses, study on the supramolecular arrangement of such ligand system is significant towards comparing the stability and reactivity towards hydrophobic protein system. The detailed crystallographic studies of four binuclear Zn Schiff bases bearing four different auxiliary groups (methyl, isopropyl, tertiary butyl and chloride), para to the phenolate Oxygen produced several intricate supramolecular structures apart from the ring and chain formations. Analysis of the methyl auxiliary group bearing dinuclear Schiff base ([Zn–Me]) shows three prominent rings and one single chain formation, excluding the intricate 3D supramolecular structure as indicated using the asymmetric unit represented in Figure 2a.

The N5 atom of the thiocyanate unit along with the acetate Oxygen atoms O2 and O5 showed formation of some significant interactions. The alternate occurrence of C14-H14B⋯N5 shown in Table 2 (forming a link between two adjacent dinuclear moiety) and an inverted ring formation of the type R_2^2 (10) (Figure S2a) involving C12-H12⋯O2 (Table 2), expanded to give a continuous linear expansion Figure 2b. These parallel sequen-ces in turn are connected via C19-H19C⋯O5 along [010] (Table 2) to form a continuous one-dimensional sheet, giving rise to a set of parallel chains of C(6) form involving C19-H19C⋯O5, perpendicular to the R_2^2 (10) ring formation as shown in Figure S2b. Columnar occurrences along [010] interlinked with the adjacent unit via the R_2^2 (10) ring formation is also observed. An R_6^6 (32) ring formed by C9-H9A⋯N5 (Table 2) and C19-H19C⋯O5 are noted (Figure S2c).

Figures 3a, b and c show the supramolecular structure of [**Zn–Me**] viewed from (011), (110) and (101) plane. On uninterrupted expansion, an intricate three-dimensional structure is obtained, and on including a slightly higher range, a C⋯C interaction is observed in Figure 3b1 forming a hexagonal tubular structure. Columnar occurrences are observed along [010] interlinked with the adjacent unit via the R_2^2 (10) ring formation along [100] almost giving it a vertebra-like structure.

The asymmetric unit (Figure 4a) of [**Zn–iPr**] comprises of two dinuclear Zn moieties, one in (011) and the other in the (110) plane along with a thiocyanate moiety. The isopropyl auxiliary group bearing system exhibited an intricate somewhat "wafer-like" formation. A C (10) chain involving C53-H53C⋯O9 (Table 3), expanded linearly when observed along [100] as shown in Figure S4a. Two such linear antiparallel chains are linked through a network of intermediary thiocyanate moieties cramming a series of alternate uninterrupted R_2^2 (12) and R_2^2 (10) rings formed by C19-H19C⋯O1 and C13-H13⋯O5 (Table 3) interactions respectively (Figures S4c–d). This sequential pattern of linkages give rise to a "sandwich formation" observed from Figure 4b. A detailed interaction of hydrogen bond for the section as marked in Figure 4b is shown in Figure 4c. However, the represented section in Figure 4c is taken as an inverted form of the alignment in Figure 4b respectively.

Figure 2. a) Asymmetric unit of [**Zn–Me**] and b) Zig zag grid like formation in the c axis involving C14-H14B⋯N5, and C12-H12⋯O2 and c) sectional view of notable hydrogen bond interactions (marked in b).

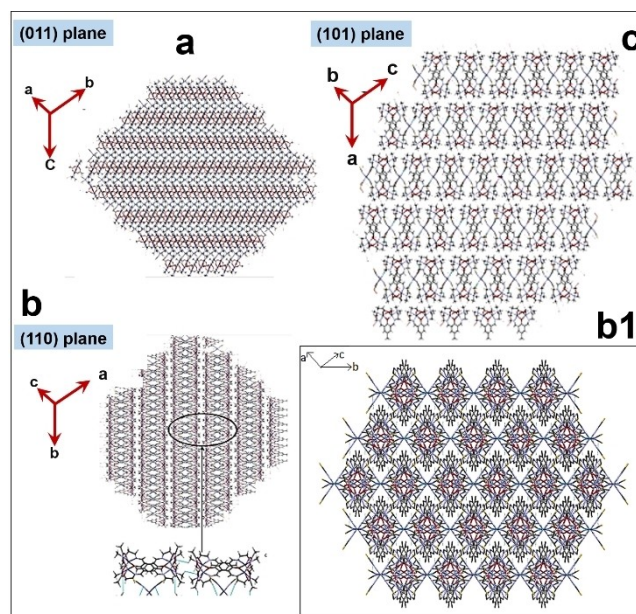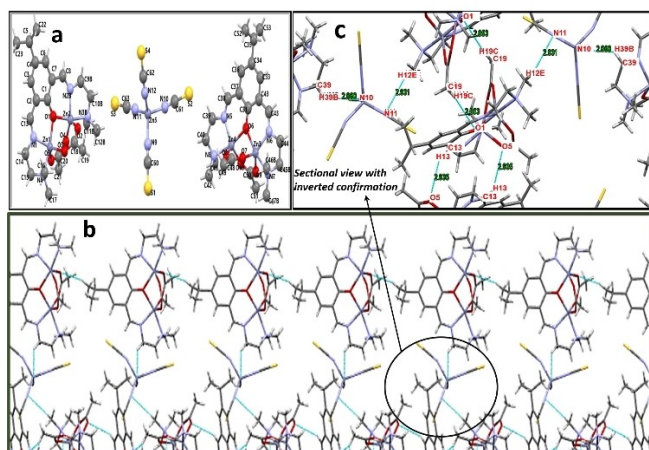| Table 2. Crystallographic details of [**Zn–Me**].			
Donor atom [D]	Acceptor atom (A)	Distance [Å]	D–H⋯A angle [°]
C14	N5	2.771	156.96
C9	N5	2.928	151.26
C19	O5	2.961	143.96
C12	O2	2.893	121.04

Figure 3. Supramolecular structure of [**Zn–Me**] viewed from a) (011), b) (110) and c) (101) plane and b1) detailed view hexagonal supramolecular structure obtained from uninterrupted expansion of [**Zn–Me**] along (110) plane.
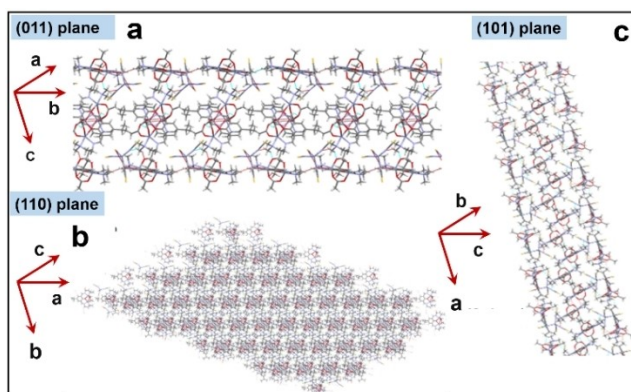
Figure 4. a) Asymmetric unit of [Zn–^{i}Pr], b) "Sandwich" or "wafer-like" formation and the corresponding magnified image (c) of the section bearing the bonds involved viewed in a perpendicular axis to the original image of [Zn–^{i}Pr].

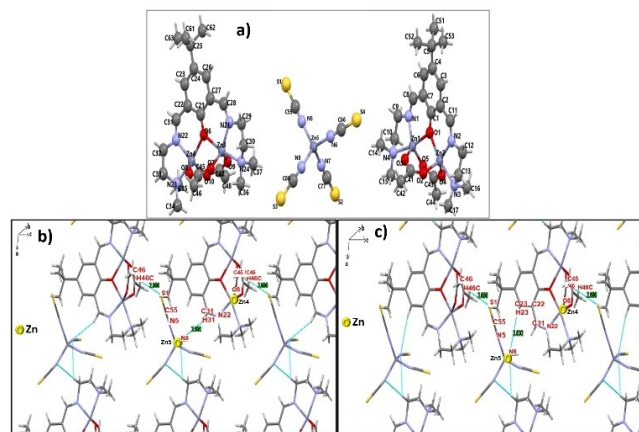**Figure 6.** a) Asymmetric unit of [Zn–^{t}Bu], b) C(13) chain involving C46-H46C···S1 with C31-H31···N8 Hydrogen bonds and c) C(15) chain involving C46-H46C···S1 with C23-H23···N8 Hydrogen bonds.

Table 3. Crystallographic details of [Zn–^{i}Pr].

Donor atom (D)	Acceptor atom (A)	Distance [Å]	D–H···A angle [°]
C39	N10	2.86	134.07
C53	O9	2.77	147.24
C44	S1	2.95	170.55
C33	N10	2.67	178.54
C12B	N11	2.93	127.89
C19	O3	2.81	144.12
C19	O1	2.85	130.49
C13	O5	2.93	123.72
C14	O1	2.99	163.19

An additional R_2^2 (10) ring involving C14-H14A···O1is also observed in [Zn–^{i}Pr] system as shown in Figure 4Sb. The three-dimensional analysis also exhibits the formation of wafer like structure which were captured along the three axes for further understanding as shown in Figure 5. In the [Zn–^{t}Bu] system (asymmetric unit shown in Figure 6a), dinuclear Zn moieties are observed one in (101) and another in (110) planes along with a thiocyanate moiety in the corresponding asymmetric unit. The

fragments along (101) plane shared a thiocyanate moiety with the one along (110) plane incorporating C23-H23···N8 and C11-H11···S1 interactions as shown in Table 4 and Figure 6Sa.
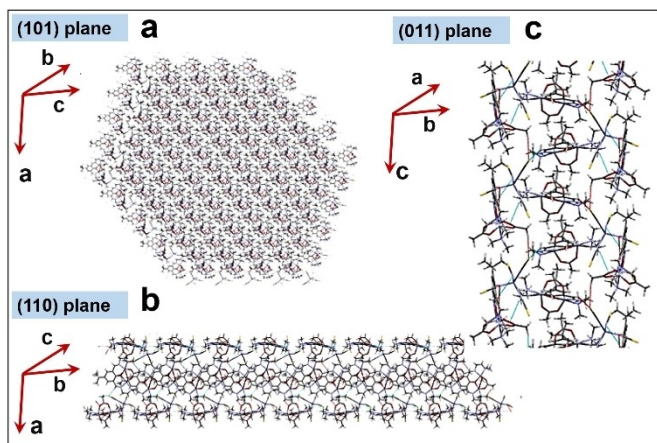
On the other hand, the bond C9-H9···O7 directly links these two macro systems as could be observed from Figure S6b. A C(12) chain (Figure S6c) is observed along [100] involving C29-H29B···N7 and C31-H31···N8 (Table 4), expanding uninterrupted as individual layers forming a flat column-like structure interconnected via C(13) and C(15) chains involving C46-H46C···S1 with C31-H31···N8 in the former (Figure 6b) and with C23-H23···N8 in the latter (Figure 6c) thereby propagating along [001] direction. In this system, too, a three-dimensional analysis resulted in a wafer formation, as observed in [Zn–^{i}Pr], which are captured along the three axes for further understanding and is represented in (Figure 7) respectively. In line of the reported studies relating to supramolecular packing in Schiff base with + I effecting compartmental ligands, Figure 8a shows the asymmetric unit of [Zn–Cl] system with the respective crystallographic details mentioned in Table 5 respectively.

Figure 5. 3D supramolecular structures of [Zn–^{i}Pr] obtained along a) (011), b) (110) and c) (101) upon uninterrupted expansion.

Table 4. Crystallographic details of [Zn–^{t}Bu].

Donor atom (D)	Acceptor atom (A)	Distance [Å]	D–H···A angle [°]
C23	N8	2.832	165.55
C11	S1	2.816	145.17
C9	O7	2.906	146.10
C29	N7	2.919	178.93
C29	N8	2.922	114.62
C31	N8	2.959	159.36
C46 [Intra]	S1	2.898	164.56

Table 5. Crystallographic details of [Zn–Cl].

Donor atom (D)	Acceptor atom (A)	Distance [Å]	D–H···A angle [°]
C5	N5	2.882	137.32
C8	N5	2.849	138.07
C20	Cl1	2.886	140.17
C10	O5	2.778	120.31
C20	O2	2.902	136.86

ChemistryOpen

Research Article
doi.org/10.1002/open.202200033
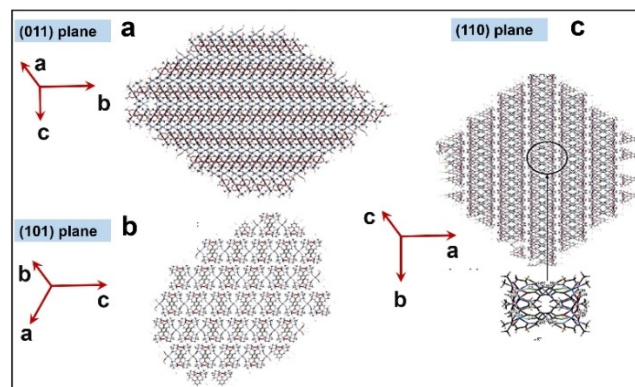
Chemistry
Europe
European Chemical
Societies Publishing

Figure 7. 3D supramolecular structures obtained along a) (101), b) (110) and c) (011) from uninterrupted expansion of [Zn–ᵗBu].

Figure 9. 3D supramolecular structures obtained along a) (011), b) (101) and c) (110) upon uninterrupted expansion of [Zn–Cl].

Figure 8. a) Asymmetric unit of [Zn–Cl] and b1), b2) & c) zig zag like formation along all three axes involving C5-H5···N5 and C20-H20A···Cl1.

The observation in this case is the study of the sequential expansion along all three axes, from a core involving an inverted ring formation of the type R_2^2 (22) (Figure S8a) via C20-H20A···Cl1 in Table 5. The progression of this ring along [100] as well as [010] both display prominent ring formations of the type R_2^2 (10) is shown in Figure S8b and comprising of C10-H10C···O5, and R_4^2 (18) (Figure S8c) involving two donor atoms of C20 and four acceptor atoms of Cl1 and O2, forming the bonds C20-H20A···Cl1 and C20-H20A···O2 (Figure S8d) respectively. The expansion along [100] however, incorporates alternating thiocyanate moieties via C5-H5···N5 and the core ring formation in an uninterrupted manner (Figure S8e). A zig zag like formation is seen in this case and has been propagating along all three axes (Figures 8b1, b2 and c) of which the formation viewed in the (110) plane gave a "vertebra"-like structure which when viewed as a three-dimensional architecture showed a column like appearance consisting of each of these vertebra-like units, each of which are interlinked via the R_2^2 (10) ring formation propagating along the [100] direction. This type of engineering is also observed involving a similar ring formation as in Figure 9. From this aforementioned
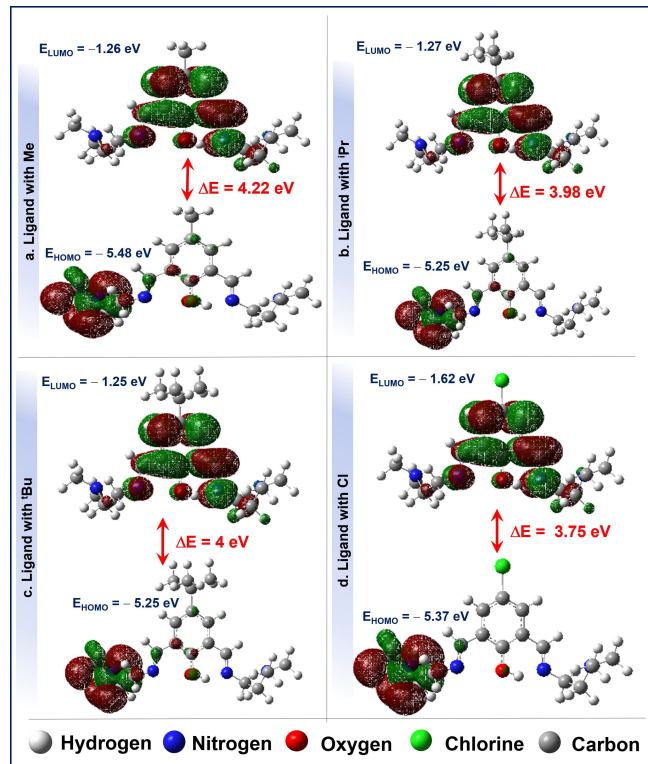
discussion, it could be therefore, stated that in spite of the unique structural aspect of the binuclear zinc(II) complex, presence of variable compartmental ligand significantly influences the intra-atomic bonding interactions and supramolecular arrangement of each zinc(II) complex. The 3D supramolecular arrangement of [Zn–Me] is found to be hexagonal arrangement (Figure 3) and being symmetric is found to be the most stable.

Detailed investigation revealed that in addition to the hydrogen bond, there exists both inter-and intra C–C bond within the system. This makes the system most stable and have least possibility to interact with the protein which is again established from the last section. In contrast to [Zn–Me], [Zn–ⁱPr] and [Zn–ᵗBu] form wafer like structure, that is, a sheet placed one on other as observed from Figures 5 and 7. Hence, compared to hexagonal structure in case of [Zn–Me], these wafers bear unbalanced force of interactions which makes them reactive with external protein like BSA. Finally, columnar vertebra, that is, epitaxy-like structure is observed in case of [Zn–Cl] (Figure 9). This structure is more fragile and thereby extent of unbalanced forces is more. This makes [Zn–Cl] to be interactive with external agents like protein in the present case. The net number of conformers of [Zn–Cl] with BSA protein is observed to be the maximum and has been described in the last section of this investigation. However, before proceeding towards molecular docking, FMO analysis of the ligand(s) with and without central zinc(II) is important. The ground state optimization and the structural feasible reactivity is required to be studied for the Schiff base as a function of variable compartmental ligands. This enables correlation of ligand reactivity with its interaction with the targeted protein.

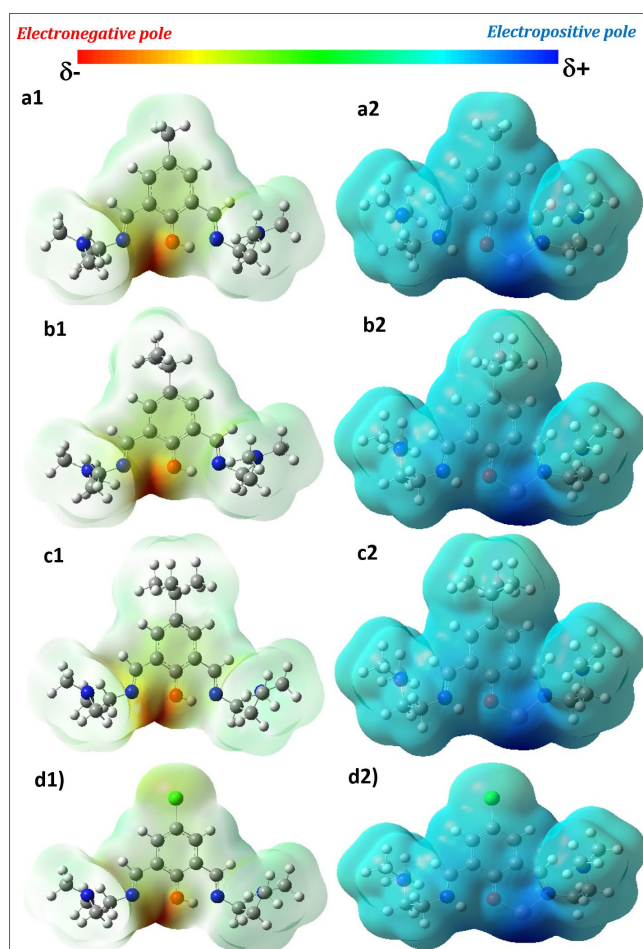## Time-Dependent Density Functional Study of the Zinc(II) Schiff Base

The initial study on crystallographic aspect of the zinc(II) Schiff base compounds is substantiated by the density functional analyses of the four systems in this section. For better understanding of the concept and bonding, the study has been reported by considering pristine ligand and metal-ligand

ChemistryOpen

Research Article
doi.org/10.1002/open.202200033

Chemistry Europe
European Chemical
Societies Publishing

complex. The ground state geometries (GSG) as well as the 3-dimensional HOMO and LUMO plots of the ligands with compartmental ligands are given in Figure 10. The respective frontier molecular orbital (FMO) of ligands along with central Zn atom is given in Figure S10 (Supporting Information). For all the derivatives, coordination with Zinc resulted in hydrogen migration to nitrogen atom. In general, HOMO and LUMO orbitals reflect the electron donor and electron acceptor part of the structure, respectively. HOMO orbitals are located on one side of the symmetrical molecule either without or with metal. On the other hand, LUMO orbital moved from phenolic part to metal moiety in metal-coordinated compounds. The docking of BSA is undertaken using only the ligand owing to which the significance of Figure 10 is discussed. It can be mentioned that, the energy gap among HOMO and LUMO is least for the ligand with Cl group. In this connection, Sen Chowdhury et al.[12] have already reported the feasibility of such zinc(II) system to get interacted with bovine serum albumin (BSA) protein in terms of spectroscopic means. This research article intends to provide a deeper and broad aspect on the influence of four compartmental ligands on the molecular docking analysis of zinc(II) Schiff base with protein systems like. BSA. In conjunction to the observations from the first section, [Zn–Me] forms the most stable hexagonal structure which also shows maximum FMO energy gap of 4.22 eV (Figure 10). This further establishes the relatively high stability of the [Zn–Me] structure. In similar manner, relatively less stable, [Zn–ⁱPr] and [Zn–ᵗBu], as predicted due to their wafer-like structure bear intermediate

FMO energy gap compared to [Zn–Me] and [Zn–Cl]. In agreement to the supramolecular fragile columnar vertebra observed in [Zn–Cl], the reactivity is predicted to be higher from comparatively lesser FMO energy gap ($\Delta E = 3.75$ eV). As expected, the FMO analyses on Zn-bonded Schiff base (Figure S10, Supporting Information) shows the influence of donation of electrons to Zn^{2+} from the parent structure wherein the FMO gap is the highest for –Cl (1.32 eV) and the least for –Me (1.29 eV) ligand. Such observation is supported by electrostatic potential maps (Figure 11) that exhibits the electron distribution throughout the structure. Red moieties indicate more electron development and blue represents lesser distribution of electronic cloud. For the metal free compounds, electron development on electronegative oxygen of hydroxyl unit is clearly indicated by the red colour. This is a good indication of coordination site with cations. Zn coordinated compounds are all blue due to donation of electrons to Zn^{2+} from the parent structure. Such observations with respect to electronic cloud distribution, HOMO/LUMO states are also supported by UV absorbance spectra obtained with TDDFT studies over the compounds and are given in Figure S11.

Figure 10. Frontier molecular orbitals (FMO) obtained from DFT calculations for ligands with compartmental groups and ligand system without central metal atom.

Figure 11. Electrostatic potential maps for: a1) Ligand with Me, a2) [Zn–Me], b1) Ligand with ⁱPr, b2) [Zn–ⁱPr], c1) Ligand with ᵗBu, c2) [Zn–ᵗBu], d1) Ligand with Cl and d2) [Zn–Cl]. The colour code used to designate the elements is similar to that in Figure 10.

It can be observed from Figure 11S that, metal free systems possess four sharp bands between 100–400 nm. However, Zn coordinated Me, ^{i}Pr and ^{t}Bu complexes show three bands while Cl has two broad bands. For all the cases, it can be seen that the peaks slightly shift towards a higher wavelength with Zn coordination irrespective of the absorption spectral range. However, the peak appeared around 200 nm is disappeared for metal free system. This can be attributed to the reduction in energy gap upon inclusion with Zn.[22] Additionally, Zn coordinated Me, ^{i}Pr, Cl and ^{t}Bu complexes show extra broad absorption peaks appeared between 400–800 nm. With this insight of study, the authors report the application of such biocompatible zinc(II) Schiff base for drug delivery agents. It could be therefore, stated that the findings from FMO support the stability for the structure of Schiff base based on the supramolecular assembly. The subsequent section is based on molecular docking of such Schiff bases with BSA protein as the ligand. These studies act as the screening for reactivity towards the macromolecular assembly as described in the section.

Molecular Docking Analyses on the Integration of Schiff Base with Variable Compartmental Ligands with Protein

The interaction/docking analyses of the experimental Schiff bases with Bovine serum albumin (BSA) is an intricate study which could be made simplified by first understanding the crystal structure of BSA. As per the literature reports,[23] the crystal structure of BSA comprises of three homologues domains marked by I, II and III as shown in Figure 12a. Each domain is further comprised of two subdomains (A and B) with respect to common structural motifs. In the present context, the primary objective being to study the interaction of BSA (PDB ID: 4F5S) with Schiff base by variation in the compartmental ligand, it is important to analyse the subdomain information which is indicated along with the amino acid sequences of BSA.[24] The interaction study is initialized through molecular docking of the BSA unit with ligand unit (without Zn being incorporated in the central part). In this connection, the nomenclature for the docked unit is framed in according to Table 1.

Irrespective of the type of compartmental ligand(s), upon considering all possible binding combinations, four distinct binding sites (Sites A, B, C and D) can be identified as highlighted in Figure 12: site A encodes a cleft of domains IB, IIIA and IIIB, site B is on the surface of domain IIA, site C is on the surface of domain IIIA, and site D is within domain IIIB. The representative statistical distribution of binding population among compartmental ligands of the parent Schiff base with four identified active sites of BSA is shown in Figure S12, from which it could be identified that site A is the most probable binding site of BSA irrespective of the variation in compartmental ligand. For each ligand, a total of 256 binding pockets are obtained from SwissDock. Each pose is further analysed in UCSF-Chimera with respect to the ΔG (Binding energy) and full fitness scores. The details of binding confirmations for the compartmental ligands with BSA as a function of spontaneity factor is shown in the plot of binding population (Figure 12S) in the Supporting Information with the cut off of $\Delta G = -7.3 \text{ kcal mol}^{-1}$ or lower. From the free energy perspective, further analysis of the complex structures reveals that the ligands L–Cl, L–^{i}Pr and L-^{t}Bu possess their strongest possible binding mode (lowest ΔG value) in site A (BSA^A–L–Cl: $\Delta G = -7.75 \text{ kcal mol}^{-1}$, Full Fitness $= -3660.4$; BSA^A–L–^{i}Pr: $\Delta G = -7.93 \text{ kcal mol}^{-1}$, Full Fitness $= -3666.4$ and BSA^A–L-^{t}Bu: $\Delta G = -8.25 \text{ kcal mol}^{-1}$, Full Fitness $= -3637.3$).

Interestingly, for L–Me the strongest binding mode is observed at site C (BSA^C–L–Me: $\Delta G = -7.62 \text{ kcal mol}^{-1}$, Full Fitness $= -3661.5$), while the same for site A is almost 0.2 kcal mol^{-1} weaker (BSA^A–L–Me: $\Delta G = -7.44 \text{ kcal mol}^{-1}$, Full
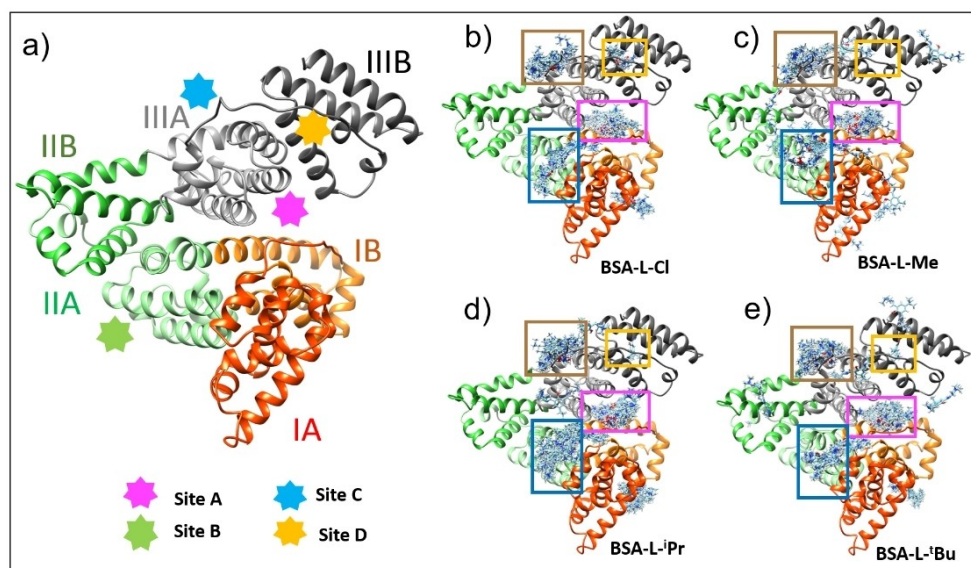

Figure 12. a) The domain structure of BSA along with its sub -domain classifications and zonal binding population density with respect to selective sites for: b) BSA–L–Cl, c) BSA–L–Me, d) BSA–L–^{i}Pr and e) BSA–L-^{t}Bu.

ChemistryOpen

Research Article
doi.org/10.1002/open.202200033

Chemistry
Europe
European Chemical
Societies Publishing

fitness$=-3662.1$). In order to gain further insight towards the interaction of the ligands with neighbouring BSA residues, a comparative study is presented in Figure 13 among the strongest interaction mode of the ligands in site A of BSA (BSA^A–L–Cl, BSA^A–L–Me, BSA^A–L–^{i}Pr and BSA^A–L–^{t}Bu). Ligplot+ has been used to analyse the binding respective interactions specifically at site A of BSA (the reason of site A selection is already discussed in the above content). The figure shows that, irrespective of the type of compartmental ligand, the interaction with cleft of site A in BSA is primarily hydrophobic in nature. However, the compartmental ligands significantly affect the selection of residue as shown in Figures 13a–d. The initial interesting interaction in case of the Schiff base with +I effecting groups (Me, ^{i}Pr and ^{t}Bu) is the hydrophobic interaction among the compartmental ligand (marked in yellow) with Arg144 residue. However, replacement of +I effecting groups

with Cl ligand promotes the hydrophobic interaction with Arg185 respectively. The compartmental ligand is also found to influence the position within the ligand cage for hydrophobic interaction with Glu424 residue as shown in Figure 13. On moving from Me to ^{i}Pr and finally to ^{t}Bu, the interaction centre with Glu424 residue changes from oxygen site to β- and δ-position respectively. Irrespective of the type of ligands, the common amino acid residue hydrophobically bonded are Ser428 [to C13 of BSA^A–L–Me, C16 of BSA^A–L–^{i}Pr, C11 of BSA^A–L–^{t}Bu and C8 of BSA^A–L–Cl], His145 [to N of BSA^A–L–Me, CH$_3$ group of BSA^A–L–^{t}Bu and C9 of BSA^A–L–Cl] and Lys114 [to C15 of BSA^A–L–Me, N of BSA^A–L–^{i}Pr and C10 of BSA^A–L–^{t}Bu]. Glu519 and Ile522 is found to have hydrophobic interaction with C15 and C12 in BSA^A–L–Me, whereas, BSA^A–L–^{i}Pr, BSA^A–L–^{t}Bu and BSA^A–L–Cl exhibit interaction with Glu424 as mentioned above. Similarly, Ile522 interacts with the α-C of N3
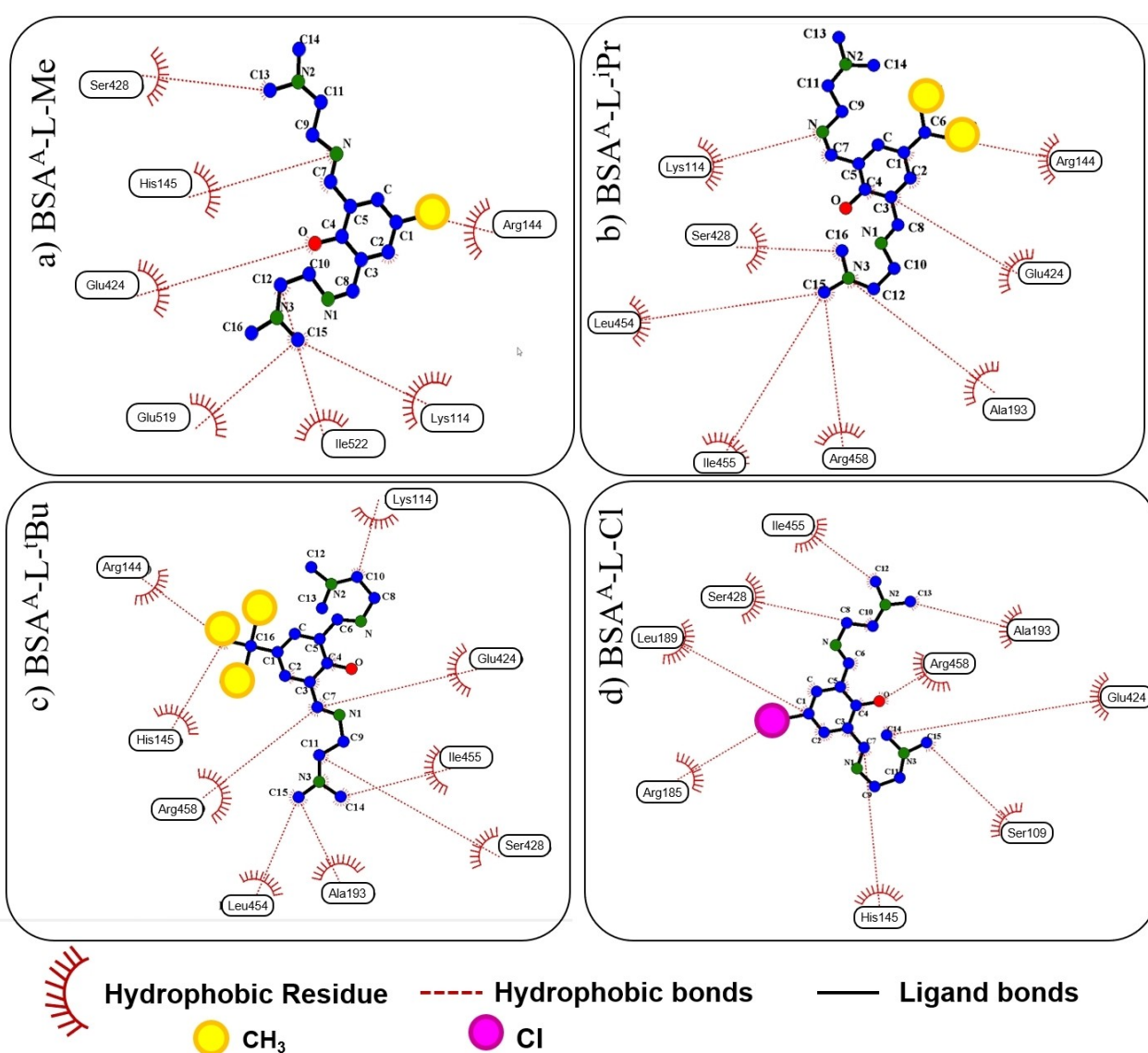
Figure 13. Detailed interaction of Schiff base with compartmental ligands with BSA. 2D representation of the docking interaction as obtained by LigPlot+ for BSA with site A with Schiff base with compartmental ligands like: a) Me, b) ^{i}Pr, c) ^{t}Bu and d) Cl. Hydrophobic interactions and the interacting protein side chain residues are shown.

ChemistryOpen

Research Article
doi.org/10.1002/open.202200033

Chemistry Europe
European Chemical
Societies Publishing

in BSA^A–L–Me and Ile455 shows hydrophobic interaction with similar α-C of N3 in BSA^A–L–^{i}Pr, BSA^A–L–^{t}Bu and BSA^A–L–Cl, respectively. The most probable interactions of protein residues with Schiff base are tabulated in Table 6 wherein four residues possess interactions with all the four Schiff bases (Me, ^{i}Pr, ^{t}Bu and Cl as compartmental ligand). In comparison to such interactions as evident for site A, site C is reported to be the most probable domain for the Schiff base with Me as the compartmental ligand. Upon changing the site, it could be noted that, variability of amino acid residue is enhanced as observed from Figure S13 in case of interaction of Schiff base with Me with site C of BSA. Arg144 residue is found to be an obvious interaction site for the +I effecting group of Schiff base in site A which is however absent for site C (for Me group in Schiff base). In this connection, the statistical distribution of the conformers (shown in the Supporting Information) is found to be least for [Zn–Me] in comparison to the [Zn–Cl] system with the highest conformers during binding with BSA. This is in agreement to the findings obtained from supramolecular analyses and also supported by FMO. From the supramolecular structure, it is studied that [Zn–Me] exists as a hexagonal supramolecular structure which is most stable with maximum FMO energy gap. This finding claims [Zn–Me] system to be least reactive with the external protein species. As expected, during binding with BSA, least conformers are reported for [Zn–Me] system with lesser spontaneity factor. In this connection, [Zn–Cl] system exist in fragile columnar vertebra with least FMO energy gap which results in maximum conformers with BSA with highest spontaneity factor (most negative ΔG). Such detailed hydrophobic interaction with BSA protein can be well correlated with the reactivity of the zinc(II) system with variable substituents as studied using FMO. Similarly, the supramolecular crystal structure of the ligand(s) gives an insight on the stability of the system which forms the basis of a pre-screening strategy for interaction with a macromolecular protein system. As already stated in the Introduction section, the authors have initially studied the binding interaction of BSA with [Zn–Me], [Zn–Cl] and [Zn–^{t}Bu] using photophysical process. However, the primary limitation lies in understanding the selective hydrophobic interaction mechanism. In absence of such study, a significant experimental endeavour is required for each protein system which is not only time consuming but cost

effective. Such study gives an insight for application of the Schiff base for acting as a drug carrier selectively and mode of interaction can be predetermined with any targeted protein residue. Study on the nature of supramolecular assembly could predict the extent of reactivity of the ligand system with targeted protein. Therefore, a pre-screening protocol could be undertaken using such theoretical research which helps in undertaking selective experiments.

Conclusion

In a nutshell, the reported research article describes the theoretical study as the primary screening tool towards application of a zinc(II) system as an Active Pharmaceutical Ingredient (API). The study is based on establishing the hydrophobic binding mechanism of the zinc(II) Schiff base with bovine serum albumin (BSA) through molecular docking. The primary ligand system is zinc(II) Schiff bases, 2,6-bis((E)-((2-(dimethylamino)ethyl)imino)methyl)-4-R-phenol, where R = methyl/tert-butyl/chloro (termed as compartmental ligand). All four systems are already reported as effective nitro aromatic detector and an initial experimental study has been carried out which proves their significant interaction with BSA. The crystallographic study of these four molecules shows the formation of supramolecular structures through hydrogen bonding and nearest neighbour interactions. The prime novelty of the present article is that, supramolecular arrangement of the ligand system could successfully predict the reactivity with a targeted protein. It acts as a pre-screening tool for selecting compartmental ligand of the Zn Schiff base for effective binding with the targeted protein. The reactivity of the system is analysed using the frontier molecular orbital (FMO) approach and substantiated with electrostatic potential maps obtained from density functional theory (DFT). The findings from the FMO approach describes the Schiff base with Methyl (Me) group to possess the highest energy gap (ΔE = 4.22 eV), thereby stabilizing the ligand and thus posing being the least reactive compared to ^{i}Pr and ^{t}Bu whose reactivities are of the same order as observed from the similar energy gap. This is in agreement to the stable hexagonal supramolecular structure obtained for [Zn–Me]. However, zinc(II) base exhibit most reactivity with Cl as the ligand having the least energy gap of 3.75 eV owing to the formation of fragile 3D columnar vertebra-like supramolecular assembly. The magnitude of HOMO-LUMO energy gap is lower for the Schiff base evaluated with zinc(II) irrespective of the type of compartmental ligand owing to the enhancement of individual HOMO and LUMO energies (e.g. E_{HOMO} and E_{LUMO} for [Zn–Me] is −11.28 eV and −9.99 eV compared to E_{HOMO} and E_{LUMO} for Ligand-Me of −5.48 eV and −1.26 eV respectively). The outcome of reactivities for such four systems are correlated with electrostatic potential maps and UV absorbance spectra obtained from TDDFT studies. Finally, as a part of pre-screening study for applicability as an API, the Schiff base ligand with four compartmental groups has been studied through molecular docking analyses using bovine serum albumin (BSA). The most stable [Zn–Me] system (predicted from

Table 6. Interaction of amino acid residues of BSA with Schiff base with variable compartmental ligands.

Amino acid residue	BSA-Ligand complexes			
	BSA^A–L–Me	BSA^A–L–^{i}Pr	BSA^A–L–^{t}Bu	BSA^A–L–Cl
Arg144	√	√	√	x
Arg185	x	x	x	√
Glu424	√	√	√	√
Glu519	√	x	x	x
Ser428	√	√	√	√
His145	√	√	√	√
Ile522	√	x	x	x
Ile455	x	√	√	√
Lys114	√	√	√	x

[a] Most probable interaction(s) are highlighted in bold.

ChemistryOpen

Research Article
doi.org/10.1002/open.202200033

Chemistry
Europe
European Chemical
Societies Publishing

supramolecular and FMO study) is observed to give least statistical distribution of conformers with lesser spontaneity factor ($-\Delta G$). In contrast, [Zn–Cl] being most reactive due to its relatively less stable 3D assembly, results in maximum population of confirmations with the highest spontaneity factor (most negative ΔG). The ligands L–Cl, L–^{i}Pr and L–^{t}Bu possess their strongest possible binding mode (lowest ΔG value) in site A. Furthermore, the hydrophobic interactions studied using 2D LigPlot+ report Arg144, Glu424, Ser428, Ile455 and Lys114 to be the most probable amino acid residues for Schiff base(s) irrespective of the type of compartment ligand whereas Arg185, Glu519, His145, Ile522 act as the differentiating residues for site A at $\Delta G = -7.3 \, \text{kcal mol}^{-1}$. These theoretical analyses based on supramolecular assembly can effectively act as the primary screening parameter for molecular docking studies of ligands with targeted protein(s). This is proposed to undertake further experimentation in terms of proper screening for application as an active pharmaceutical ingredient.

Acknowledgements

Conflict of Interest

The authors declare no conflict of interest.

Data Availability Statement

The data that support the findings of this study are available from the corresponding author upon reasonable request.

[1] A. Rauf, A. Shah, K. S. Munawar, A. A. Khan, R. Abbasi, M. A. Yameen, A. M. Khan, A. R. Khan, I. Z. Qureshi, H. B. Kraatz, Z. U. Rehman, *J. Mol. Struct.* **2017**, *1145*, 132–140.

[2] M. Khoutoul, M. Lamsayah, F. F. Al-blewi, N. Rezki, M. R. Aouad, M. Mouslim, R. Touzani, *J. Mol. Struct.* **2016**, *1113*, 99–107.

[3] L. Q. Chai, J. Y. Zhang, L. C. Chen, Y. X. Li, L. J. Tang, *Res. Chem. Intermed.* **2016**, *42*, 3473–3488.

[4] M. Jafari, M. Salehi, M. Kubicki, A. Arab, A. Khaleghian, *Inorg. Chim. Acta* **2017**, *462*, 329–335.

[5] D. Majumdar, D. Das, S. S. Sreejith, S. Das, J. K. Biswas, M. Mondal, D. Ghosh, K. Bankura, D. Mishra, *Inorg. Chim. Acta* **2019**, *489*, 244–254.

[6] Q. Poladian, O. Şahin, T. Karakurt, B. İlhan-Ceylan, Y. Kurt *Polyhedron* **2021**, *201*, 115164.

[7] A. Guelai, H. Brahim, A. Guendouzi, M. Boumediene, S. Brahim, *J. Mol. Model.* **2018**, *24*, 301.

[8] K. G. Vladimirova, A. Y. Freidzon, O. V. Kotova, A. A. Vaschenko, L. S. Lepnev, A. A. Bagatur'yants, M. V. Alfimov, *Inorg. Chem.* **2009**, *48*, 11123–11130.

[9] S. K. Loke, E. Pagadala, V. Srinivasadesikan, V. R. J. R. S. Thanapaul, T. Pooventhiran, R. Thomas, G. Naganjaneyulu, R. K. Kottalanka, *Inorg. Chem. Commun.* **2021**, *133*, 108936.

[10] A. Ramesh, R. Pawar, P. Shyam, A. Ramachandraiah, *Res. Chem. Intermed.* **2021**, *47*, 4673–4697.

[11] S. Dasgupta, E. Zangrando, I. Majumder, *ChemistrySelect* **2017**, *2*, 1.

[12] M. Sen Chowdhury, A. Sarkar, S. R. Rai, S. Dasgupta, I. Majumder, A. Bhattacharya, D. Das, D. Bose, J. Mukhopadhyay, M. Mukhopadhyay, *Appl. Organomet. Chem.* **2021**, *35*, e6164.

[13] D. Escudero, A. Laurent, D. Jacquemin in *Handbook of Computational Chemistry* (Eds. J. Leszczynski, A. Kaczmarek-Kedziera, T. Puzyn, M. G. Papadopoulos, H. Reis, M. K. Shukla) Springer, Cham **2017**.

[14] L. H. Al-Wahaibi, J. Joubert, O. Blacque, N. H. Al-Shaalan, A. A. El-Emam, *Sci. Rep.* **2019**, *9*, 19745.

[15] A. Ruiz, H. Pérez, C. Morera-Boado, L. Almagro, C. C. P. da Silva, J. Ellena, J. M. G. de la Vega, R. Martínez-Alvarez, M. Suárez, N. Martín, *CrystEngComm* **2014**, *16*, 7802.

[16] K. Karthikeyana, I. Ramab, A. Subashinib, C. Arunagiric, S. Selvakumar, *Chem. Data Collect.* **2020**, *25*, 100337.

[17] M. J. Frisch, G. W. Trucks, H. B. Schlegel, G. E. Scuseria, M. A. Robb, J. R. Cheeseman, G. Scalmani, V. Barone, G. A. Petersson, H. Nakatsuji, X. Li, M. Caricato, A. V. Marenich, J. Bloino, B. G. Janesko, R. Gomperts, B. Mennucci, H. P. Hratchian, J. V. Ortiz, A. F. Izmaylov, J. L. Sonnenberg, D. Williams-Young, F. Ding, F. Lipparini, F. Egidi, J. Goings, B. Peng, A. Petrone, T. Henderson, D. Ranasinghe, V. G. Zakrzewski, J. Gao, N. Rega, G. Zheng, W. Liang, M. Hada, M. Ehara, K. Toyota, R. Fukuda, J. Hasegawa, M. Ishida, T. Nakajima, Y. Honda, O. Kitao, H. Nakai, T. Vreven, K. Throssell, J. A. Montgomery, Jr., J. E. Peralta, F. Ogliaro, M. J. Bearpark, J. J. Heyd, E. N. Brothers, K. N. Kudin, V. N. Staroverov, T. A. Keith, R. Kobayashi, J. Normand, K. Raghavachari, A. P. Rendell, J. C. Burant, S. S. Iyengar, J. Tomasi, M. Cossi, J. M. Millam, M. Klene, C. Adamo, R. Cammi, J. W. Ochterski, R. L. Martin, K. Morokuma, O. Farkas, J. B. Foresman, D. J. Fox, Gaussian, Inc., Wallingford CT, **2016**.

[18] A. D. Becke *Phys. Rev. A* **1988**, *38*, 3098–3100.

[19] C. Lee, W. Yang, R. G. Parr, *Phys. Rev. B* **1988**, *37*, 785–789.

[20] A. Grosdidier, V. Zoete, O. Michielin, *Nucleic Acids Res.* **2011**, *39*, W270-W277.

[21] E. F. Pettersen, T. D. Goddard, C. C. Huang, G. S. Couch, D. M. Greenblatt, E. C. Meng, T. E. Ferrin, *J. Comput. Chem.* **2004**, *25*, 1605–12.

[22] B. J. Nagare, S. Chavan, V. Bambole, *Mat. Res. Exp.* **2017**, *4*, 106304.

[23] S. Curry, H. Mandelkow, P. Brick, N. Franks, *Nature Struct. Biol.* **1998**, *5*, 827–835.

[24] B. X. Huang, H. Y. Kim, C. Dass, *J. Am. Soc. Mass Spectrom.* **2004**, *15*, 1237–47.